ELSEVIER

Solid State Ionics 135 (2000) 643–651

SOLID STATE IONICS

www.elsevier.com/locate/ssi

Electronic transport properties and electronic structure of TiO_2-doped YSZ

Kiyoshi Kobayashi[a,*], Shu Yamaguchi[a], Toru Higuchi[b], Shik Shin[c], Yoshiaki Iguchi[a]

[a]*Department of Materials Science and Engineering, Nagoya Institute of Technology, Gokiso-cho, Showa-ku, Nagoya 466-8555, Japan*
[b]*Facility of Science, Science University of Tokyo, Kagurasaka 1-3, Shinjuku, Tokyo 162-0825, Japan*
[c]*Institute of Solid State Physics, University of Tokyo, Tanashi 188-8501, Japan*

Abstract

Electronic conductivity of yttria-stabilized zirconia (YSZ) doped with 2 mol% of TiO_2 was measured by the dc-polarization technique using the Hebb–Wagner's asymmetric cell. The X-ray absorption spectroscopy (XAS) was also employed for 2, 5 and 10 mol% of TiO_2-doped YSZ in order to investigate the electronic structure near the band gap. The partial conductivity of conduction electrons equilibrated at unit oxygen partial pressure (σ_n°) increased with increasing TiO_2 concentration and the apparent activation energy of σ_n° decreased by the TiO_2 doping. In contrast, the partial conductivity of holes and the apparent activation energy were almost independent of TiO_2 concentration. These results suggest the band-gap narrowing by TiO_2 doping, which is consistent with the results of the X-ray absorption spectroscopy measurements, where unoccupied t2g states of Ti3d below the conduction band grew with the increase of the TiO_2 concentration. The change in the electronic conductivity with TiO_2 concentration was discussed based on the percolation theory.

Keywords: TiO_2-doped yttria-stabilized zirconia; Mixed conductor; Electronic conductivity; Dc-polarization; XAS

Materials: TiO_2-doped yttria stabilized zirconia; YSZ; TiO_2

1. Introduction

Mixed electronic and oxide ion conductor has attracted attentions due to potential applications as anode materials in solid oxide fuel cell, gas separators for oxygen, and other electrochemical devices for energy conversion systems [1]. Among potential candidates, titania-doped yttria stabilized zirconia (TD-YSZ) has been focused on since the report on the mixed conductivity by Liou and Worrell [1]. Although enhancement of the partial conductivity of electrons (σ_n°) by the TiO_2 doping to yttria-stabilized zirconia has been observed by total conductivity measurements [2–4] and electronic conductivity measurements by the dc-polarization technique using Hebb–Wagner's asymmetric cell [5,6], no experimental evidence has been given for the explanation of enhanced electronic conductivity by the TiO_2 doping.

With regard to the influence of the electronic structures of TD-YSZs, narrowing of the band-gap

*Corresponding author. Present address: National Institute of Materials and Chemical Research, Higashi 1-1, Tsukuba 305-8565, Japan. Fax: +81-298-61-4709.

E-mail address: kiyoshi@nimc.go.jp (K. Kobayashi).

0167-2738/00/$ – see front matter
PII: S0167-2738(00)00426-4

(E_g) was observed by the electron energy loss spectroscopy (EELS) and ultraviolet photoelectron spectroscopy (UPS) [7], which also suggested that no effect of O2p states on the TiO_2 doping to YSZ within the solid solubility limit.

The percolation model has been proposed in order to explain the enhancement of the electronic conductivity by the TiO_2 doping from the electrochemical measurements [8]. Employing this model, activation energy for the conduction of electrons have to show a drastic change at the TiO_2 concentration of percolation threshold. In this paper, for the purpose of the investigation about the validity of the percolation model and discussion on the cause of enhancement for the electronic conductivity by the TiO_2 doping, the electronic conductivity measurements of 2 mol% TiO_2-doped YSZ have been made using the dc-polarization method in addition to the results of previous reports for the electronic conductivities of 5 and 10 mol% TiO_2-doped YSZ [5,6]. Furthermore, X-ray absorption spectroscopy (XAS) was measured for 2, 5 and 10 mol% of TiO_2-doped yttria-stabilized zirconia to clarify the effects of the TiO_2 doping to YSZ on the electronic structure near the conduction band.

2. Experimental

2.1. Dc-polarization measurements

Dc-polarization measurements of 2 mol% TiO_2-doped yttria stabilized zirconia (denoted as 2TD-YSZ hereinafter) were made using the disk-shaped sample synthesized by a conventional solid-state reaction method. Starting materials are 8 mol% yttria-stabilized zirconia powder with 99.9% purity supplied by Tosoh Co. Ltd. (Tokyo, Japan) and TiO_2 with 99.99% purity supplied by Rare Metallic Co. Ltd. (Tokyo, Japan). Nominal composition of the sample was expressed as $Zr_{0.835}Y_{0.145}Ti_{0.02}O_{1.927}$.

Dc-polarization cell used in this study is shown in Fig. 1. The blocking electrode was fabricated using the gold plate, alumina disk, and Pyrex glass gasket. The experimental procedures for the dc-polarization measurements were almost identical to the previous report [5]. The measurements were made at 1273, 1223, 1173, 1123 and 1073 K. Oxygen fugacity, P_{O_2}, at the reversible electrode side ($P^{rev}_{O_2}$) was fixed at 1.0 by flowing the oxygen gas. The authors defined the oxygen fugacity as $P_{O_2} = (p_{O_2}/\text{Pa})/(P^{\ominus}/\text{Pa})$, where $P^{\ominus}$ is the standard pressure of 1.013×10^5 Pa. The potentiostatic dc voltage, E_{app}, ranging from 0.3 to 1.7 V was applied between the reversible electrode and blocking electrode, and the value of external current, i_{ext}, was recorded after the steady state was achieved.

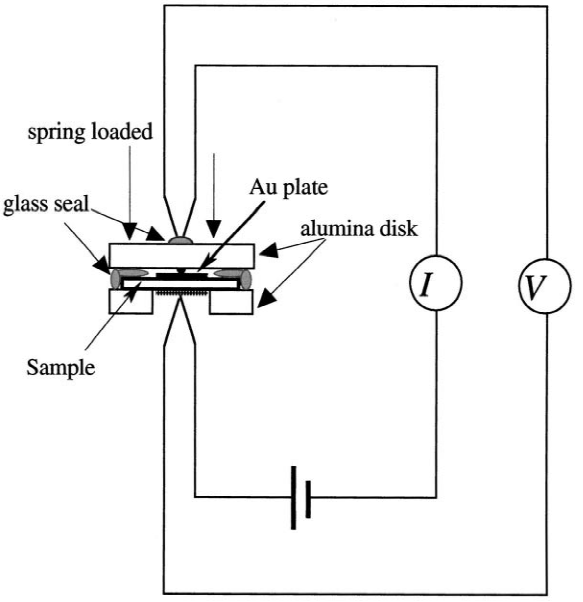

Fig. 1. Schematic illustration of the dc-polarization cell used for the electronic conductivity measurements of 2TD-YSZ.

2.2. X-ray absorption spectroscopy measurements

The X-ray absorption spectroscopy (XAS) was carried out at undulator beamline BL-19B in the Photon Factory at High Energy Accelerator Research Organization, Tsukuba, in Japan. Synchrotron radiation from the undulator was monochromatized using a grating monochrometer VLM19. The resolution of the beamline was smaller than about 50 meV at $h\nu = 500$ eV. The XAS spectra were measured by the XUV silicon photodiode.

The XAS measurements were made for 2TD-YSZ, 5 mol% TiO_2-doped YSZ (denoted as 5TD-YSZ), and 10 mol% TiO_2-doped YSZ (10TD-YSZ). Before the measurements, the samples were annealed at

1873 K for 10 h in air to obtain the single fluorite phase [9].

3. Results

3.1. Electronic conductivity

Typical results of the dc-polarization measurements between 1073 and 1273 K under $P_{O_2}^{rev} = 1.0$ are shown in Fig. 2. Values of i_{ext} are almost independent of E_{app} below 1.0 V, while the rapid increase of i_{ext} with increasing E_{app} is found in the region between 1.0 and 1.7 V. Total electronic conductivity, $\sigma_e^{block} (= \sigma_n^{block} + \sigma_p^{block})$, under oxygen fugacity at the blocking electrode, $P_{O_2}^{block}$, and the partial conductivities of electrons and holes, σ_n and σ_p equilibrated at $P_{O_2}^{rev}$ can be calculated from the following relationships [10,11]. Detailed calculation procedures using the following relationships have been discussed in the previous reports [5],

$$\sigma_e^{block} = \frac{L}{A}\frac{\partial i_{ext}}{\partial E_{app}} = \frac{L}{A} i_{ext} \frac{\partial \ln i_{ext}}{\partial E_{app}}, \quad (1)$$

and

$$i_{ext} = \frac{RTA}{L}\left\{\sigma_n^*\left(\exp\left[\frac{E_{app}F}{RT}\right]\right) + \sigma_p^*\left(\exp\left[-\frac{E_{app}F}{RT}\right]\right)\right\}, \quad (2)$$

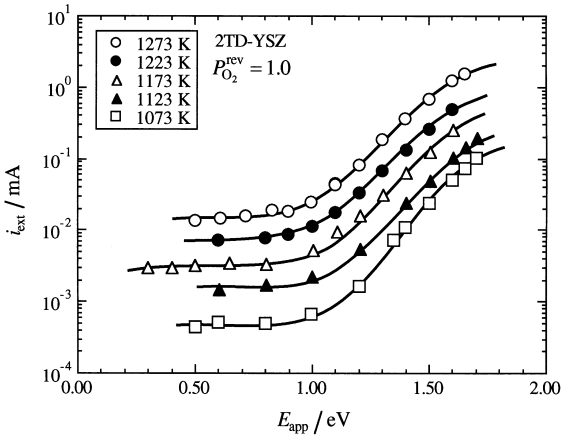

Fig. 2. Relationship between applied voltage, E_{app}, and steady-state external current, i_{ext}, of 2TD-YSZ at 1273, 1223, 1173, 1123 and 1073 K under $P_{O_2}^{rev} = 1.0$.

where, L and A are the thickness of sample and the electrode area. R and T are gas constant and Faraday constant, and σ_n^* and σ_p^* are the partial conductivities of electrons and holes in equilibrium with $P_{O_2}^{rev}$, respectively. Relationship between E_{app} and $P_{O_2}^{block}$ is also given by the Nernst equation as,

$$E_{app} = \frac{RT}{4F} \ln \frac{P_{O_2}^{block}}{P_{O_2}^{rev}}. \quad (3)$$

Variation of the $\log \sigma_e$, $\log \sigma_n$ and $\log \sigma_p$ with $\log P_{O_2}$ calculated using the Eqs. (1)–(3) are illustrated in Fig. 3. Similar to the 5TD- and 10TD-YSZ, σ_n and σ_p are proportional to $P_{O_2}^{-1/4}$ and $P_{O_2}^{1/4}$, respectively, in the region of $\log P_{O_2} \geq -20$, while the deviation of $P_{O_2}^{-1/4}$ proportionality was found at low P_{O_2} region. One possible explanation of the deviation of the $P_{O_2}^{-1/4}$ proportion is the effect of non-ohmic contact at solid electrolyte/blocking electrode interface, so-called Schottky barrier [12,13].

3.2. X-ray absorption spectra

O1s X-ray absorption spectra of 2TD-, 5TD- and 10TD-YSZ are shown in Fig. 4. In the lightly 3d and 4d transition metal compounds, the dipole selection rules indicate that the O1s XAS spectra correspond to transitions into O2p character hybridized into the

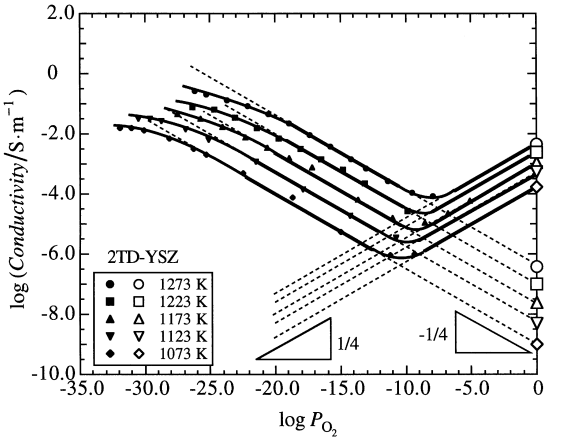

Fig. 3. Variations of $\log \sigma_e$ (closed symbol with solid curve form the slope of the polarization curve in Fig. 2), $\log \sigma_n$ and $\log \sigma_p$ (shown by the open symbol determined from Eq. (2)) with $\log P_{O_2}$ for 2TD-YSZ.

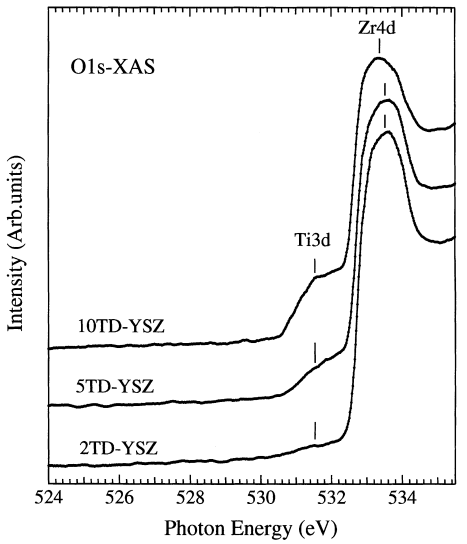

Fig. 4. O1s X-ray absorption spectra of 2TD-, 5TD- and 10TD-YSZ.

unoccupied metal states. The peak at ~531.5 eV is the t2g subband of the unoccupied Ti3d states. The peak at ~533.5 eV is the t2g subband of the unoccupied Zr4d states. The eg subbands of Zr4d and Ti3d states which are located at higher energy side are not shown in this figure, because electronic transport properties are not affected by the eg subbands.

4. Discussion

4.1. Defect model

As described in the previous reports [4–6], the experimental condition of the polarization measurements is in the extrinsic defect predominant region, where the oxygen vacancy formed by the charge compensation of Y^{3+} replacing $(Zr/Ti)^{4+}$ ion is predominating defect. The quasi-chemical reaction of oxygen vacancy formation can be written using the Kröger–Vink notation [14] as,

$$O_O^{\times} = \frac{1}{2}O_2 + V_O^{\cdot\cdot} + 2e', \qquad (A)$$

where $O_O^{\times}$ and $V_O^{\cdot\cdot}$, and e' are neutral oxide ion on the normal sites, oxide ion vacancy, and free electron, respectively. The equilibrium constant of Eq. (A), $K_{V_O^{\cdot\cdot}}$, is also given using the concentration of $V_O^{\cdot\cdot}$ ($[V_O^{\cdot\cdot}]$) and e' (n) as following,

$$K_{V_O^{\cdot\cdot}} = [V_O^{\cdot\cdot}]n^2P_{O_2}^{1/2} = K^{\circ}_{V_O^{\cdot\cdot}} \exp\left(-\frac{\Delta H_{V_O^{\cdot\cdot}}}{KT}\right), \qquad (4)$$

where $K^{\circ}_{V_O^{\cdot\cdot}}$ and $\Delta H_{V_O^{\cdot\cdot}}$ are the constant including the entropy term and enthalpy change of Eq. (A), respectively. The intrinsic ionization reaction,

$$0 = e' + h^{\cdot}, \qquad (B)$$

yields the following relationship using the concentration of electrons, holes and the equilibrium constant for the reaction (B), K_i, as,

$$K_i = np = K_i^{\circ} \exp\left(-\frac{\Delta H_i}{kT}\right), \qquad (5)$$

where $h^{\cdot}$ and p are free holes and the concentration of $h^{\cdot}$, respectively, and ΔH_i and K_i° are enthalpy change of the reaction (B) and the constant, respectively.

The Ti^{3+} ions reduced from Ti^{4+} ions are formed at high temperature under low P_{O_2} condition, since quenched samples equilibrated at 1273 K under $\log P_{O_2} = -18$ are blackened. The Ti^{3+} formation reaction and the equilibrium constant, K_{Ti} are given as following,

$$Ti_{Zr}^{\times} + e' = Ti_{Zr}', \qquad (C)$$

and

$$K_{Ti} = \frac{[Ti_{Zr}']}{[Ti_{Zr}^{\times}]n}, \qquad (6)$$

where $Ti_{Zr}^{\times}$ and Ti_{Zr}' are the neutral titanium ion on the zirconium sites and singly negative-charged titanium ion on zirconium sites, and $[Ti_{Zr}^{\times}]$ and $[Ti_{Zr}']$ are the concentration of $Ti_{Zr}^{\times}$ and Ti_{Zr}', respectively. From Eq. (6), $[Ti_{Zr}']$ is given by

$$[Ti_{Zr}'] = K_{Ti}[Ti_{Zr}^{\times}]n. \qquad (6\text{-}1)$$

As discussed previously, $[Ti_{Zr}']$ is much lower than $[Ti_{Zr}^{\times}]$ in P_{O_2} range of this experimental condition [4]. In this case, $[Ti_{Zr}^{\times}]$ is approximately equal to the initial doped concentration of TiO_2. Therefore, P_{O_2} dependency of n is not affected by Ti_{Zr}' formation.

The overall electrical neutrality condition is approximately given as following,

$$[Y'_{Zr}] \approx 2[V_O^{\cdot\cdot}] \gg n,\ p,\ [Ti'_{Zr}]. \quad (7)$$

Combination of Eqs. (4)–(7), n and p can be expressed as,

$$n = K^{\circ}_{V_O^{\cdot\cdot}} \left(\frac{2}{[Y'_{Zr}]}\right)^{1/2} \exp\left(-\frac{\Delta H_{V_O^{\cdot\cdot}}/2}{kT}\right) P_{O_2}^{-1/4}, \quad (8)$$

and

$$p = \frac{K^{\circ}_{i}}{K^{\circ}_{V_O^{\cdot\cdot}}} \left(\frac{2}{[Y'_{Zr}]}\right)^{1/2} \exp\left(-\frac{\Delta H_i - \Delta H_{V_O^{\cdot\cdot}}/2}{kT}\right) P_{O_2}^{1/4}. \quad (9)$$

Partial conductivities of electrons and holes can be given using the mobilities of electrons and holes (μ_n and μ_p) as,

$$\sigma_j = e\mu_j\, j,\ (j = n,\ p), \quad (10)$$

where e is the unit electronic charge. Because of the reasonable assumption that mobilities of electrons and holes (μ_n and μ_p) are independent of P_{O_2}, the σ_n and σ_p are expected as being proportional to $P_{O_2}^{-1/4}$ and $P_{O_2}^{1/4}$, respectively.

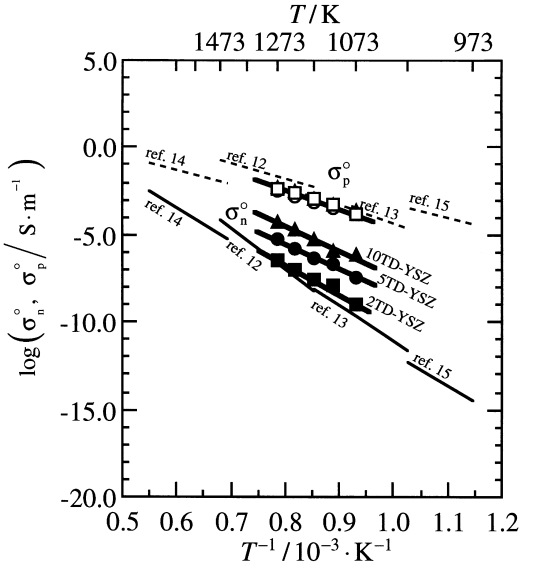

Fig. 5. Arrhenius plots of the partial conductivities for electrons and holes at $P_{O_2}=1.0$, σ°_n and σ°_p, for 2TD-, 5TD- [5] and 10TD-YSZ [6]. The results of non-doped YSZ [15–17] and yttria partial stabilized zirconia [18] are also plotted for comparison.

4.2. Estimation of the band-gap

Arrhenius plots of the partial conductivities for σ_n and σ_p at $P_{O_2}=1.0$, σ°_p and σ°_n, are shown in Fig. 5 together with those of non-doped YSZ [15–17], yttria partially stabilized zirconia [18], 5TD-YSZ [5] and 10TD-YSZ [6]. σ°_n increased with increasing TiO_2 concentration, while σ°_p is almost independent of TiO_2 concentration. The same tendency of the temperature and TiO_2 concentration for σ°_n and σ°_p has been reported for TiO_2–Y_2O_3-stabilized polycrystalline tetragonal zirconia [19]. The apparent activation energies for σ°_n, E_{an}, calculated from the slope of the Arrhenius plots decreased by the TiO_2 doping, while that of σ°_p, E_{ap}, is almost independent of TiO_2 concentration. E_{an} and E_{ap} are related to the $\Delta H_{V_O^{\cdot\cdot}}$, ΔH_i, and activation energies of μ_n and μ_p (E_{μ_n} and E_{μ_p}) from Eqs. (8)–(10)

$$E_{an} = \frac{\Delta H_{V_O^{\cdot\cdot}}}{2} + E_{\mu_n} \quad (10)$$

and

$$E_{ap} = \Delta H_i - \frac{\Delta H_{V_O^{\cdot\cdot}}}{2} + E_{\mu_p}. \quad (11)$$

The physical meaning of E_{an} is the activation energy for the formation of one electron in the oxides with the assumption that the E_{μ_n} value is small enough compared to the value of $\Delta H_{V_O^{\cdot\cdot}}/2$. E_{an} values of 5TD- and 10TD-YSZ are calculated to be 2.80 and 2.73 eV, respectively, which are close to the value of TiO_2 with rutile structure (2.2 eV) [20].

The band-gap between conduction and valence band, E_g, can be also estimated from sum of Eqs. (10) and (11) as,

$$E_{an} + E_{ap} = E_g + E_{\mu_n} + E_{\mu_p}, \quad (12)$$

because ΔH_i is identical to E_g. If the values of E_{μ_n} and E_{μ_p} were independent of x, the dependence of the $E_{an}+E_{ap}$ corresponds to the E_g dependence on x from Eq. (12). From the experimental results, the value of $E_{an}+E_{ap}$ for non-doped YSZ has been reported to be close to the E_g value estimated by the optical method, and therefore, the E_g suggested to be estimated by $E_{an}+E_{ap}$, which is presented as E^{σ}_g hereinafter, in this paper. Variation of the E^{σ}_g with

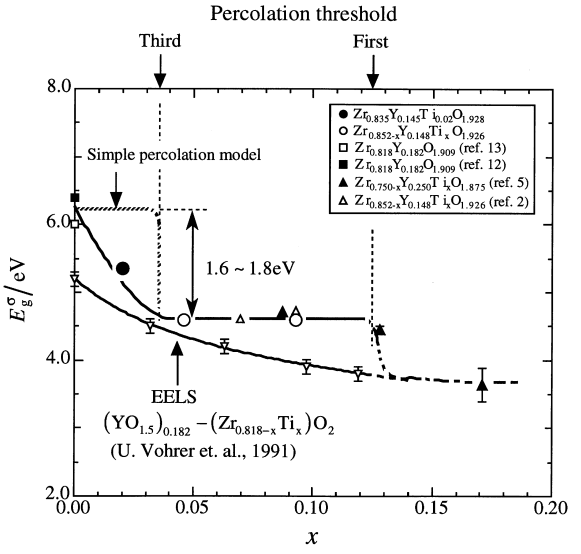

Fig. 6. Variation of E_g^σ with molar fraction of TiO_2 in TD-YSZs, x, calculated from the dc-polarization and total conductivity measurements. The relationship between the band-gap, E_g, and x in $(YO_{1.5})_{0.182}-(Zr_{0.818-x}Ti_x)O_2$ estimated by the electron energy loss spectra [21] is also plotted for comparison.

molar fraction of TiO_2, x, is illustrated in Fig. 6. The E_{an} values of TD-YSZs with x higher than 0.07 can be calculated from the total conductivities [2,4]. E_g^σ plotted in Fig. 6 were estimated by assuming the constant value for E_{ap} of 1.87 eV for the sample of $x \geq 0.07$, which was the average E_{ap} value of 2TD-, 5TD- and 10TD-YSZ. The E_g values obtained from the EELS measurements [21] are also plotted for comparison. The E_g^σ values are found to depend on x only and independent of $YO_{1.5}$ concentration as shown in Fig. 6.

Gap energy between Zr4d states and Ti3d states (ΔE) in YSZ doped with 150 ppm of TiO_2 measured by the coloration method has been suggested as 1.8 eV [22], and the ΔE value is found to be close to the difference between the E_g^σ values of non-doped YSZ and the values of 5TD- and 10TD-YSZ (1.6–1.8 eV) as shown in Fig. 6. Ti3d states in YSZ doped with 150 ppm of TiO_2 are suggested to work as a localized electron-trapping level and, therefore, the E_g^σ value of YSZ doped with 150 ppm of TiO_2 is suggested to be the same with the value of non-doped YSZ [22]. On the other hand, E_g^σ values of 2TD-, 5TD- and 10TD-YSZ decreased by the increase in TiO_2 concentration. Hence, electronic structure of the conduction band in TD-YSZ is suggested to be different from that of non-doped YSZ in high TiO_2 concentration region.

Assuming that the electrons in the Ti3d states and holes in O2p states in TD-YSZs are in thermal equilibrium through the intrinsic ionization reaction given by Eq. (B), the E_g^σ values of 5TD- and 10TD-YSZ are suggested to be about 2.0 eV smaller than the E_g^σ value of non-doped YSZ estimated from the difference of the lower edges for Zr4d and Ti3d states shown in Fig. 4. Both of the E_g^σ values calculated from the electronic conductivity measurements and O1s-XAS measurements are found to show good agreements with each other, and the main reason for the enhancement of the partial conductivity of electrons is suggested to be the narrowing of band-gap by the Ti3d band below the lower edge of the Zr4d states.

4.3. Percolation model

As shown in Fig. 6, the variation of the E_g^σ with x can be distinguished into three regions; (I) concentration region of $0<x<0.04$ where the E_g^σ values are continuously decreased with increasing x; (II) the region of $0.04<x<0.13$ where the E_g^σ values are almost independent of x; and (III) further decrease of E_g^σ with increasing x is shown in $x>0.13$ region. The x dependence of E_g^σ can be explained using a percolation model as follows.

The bond percolation threshold (P_c) for fcc structure which corresponds to the cation coordination in fluorite structure is approximately given using the site coordination number, Z, as follow [8],

$$ZP_c = 1.5 \quad (13)$$

Using this relationship, threshold values of x for the formation of Ti ion network of third, second, and first nearest neighbors (x_{III}, x_{II}, x_I) are 0.036, 0.05 and 0.125, respectively. The values of the boundary concentrations at region (I)/(II) and region (II)/(III) show good agreement with x_{III} and x_I, respectively.

Variation of E_g^σ with x estimated from the simple percolation model with the assumption e′ that can migrate through Ti–O bonds is also plotted in Fig. 6. From this model, the E_g^σ should be almost independent of x below 0.036 because Ti^{3+} ions are isolated.

It should be noted that Ti^{3+} ions are not identified by analysis of the electron paramagnetic resonance (EPR) for YSZ with various amounts of TiO_2 equilibrated between 893 and 1133 K from $P_{O_2} = 10^{-17}$ to 10^{-11} [8]. However, x dependency of E_g^{σ} estimated by the simple percolation model shows the disagreement with the experimental results as shown in Fig. 6.

In order to explain the variation of the E_g^{σ} with x obtained in this study, the modified percolation

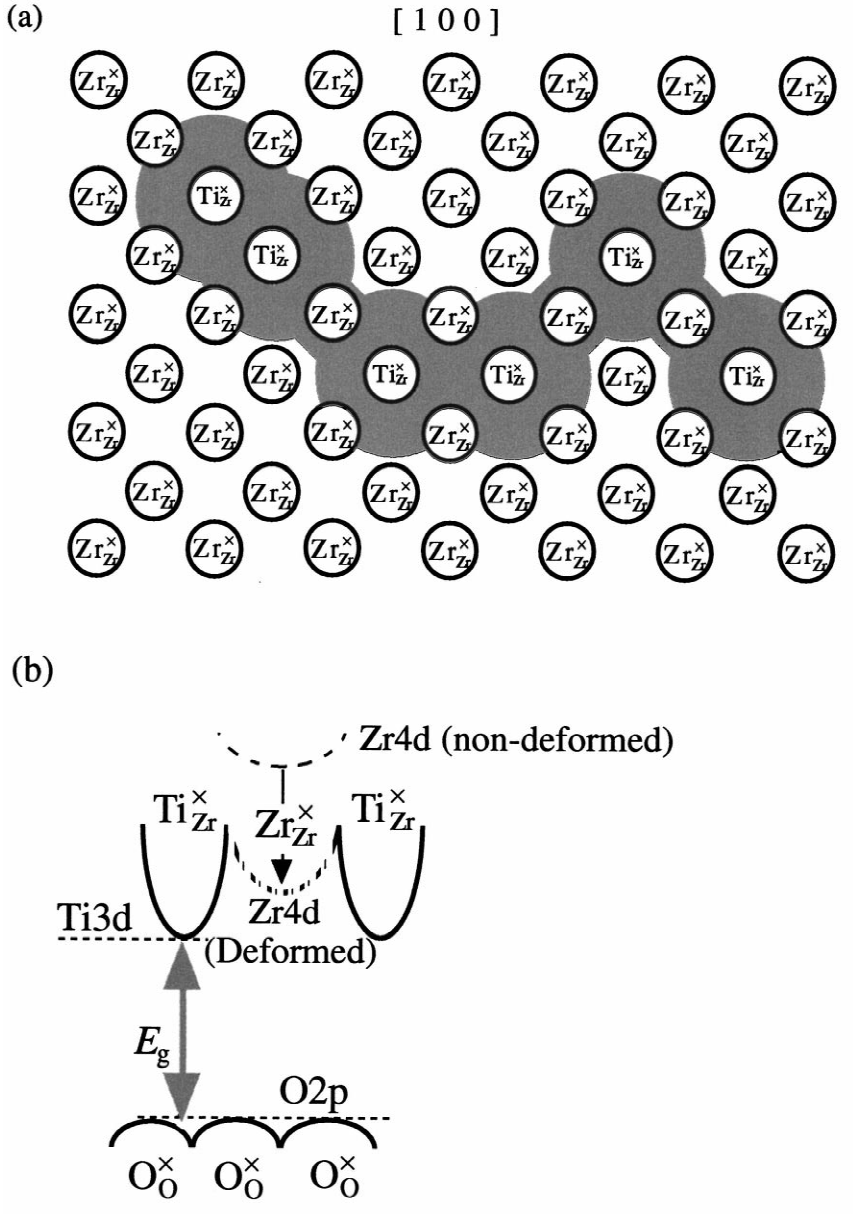

Fig. 7. Schematic illustration of (a) the cation coordination on (100) plane and (b) the electronic structure in this path. Percolation path of second and third nearest neighbors are also shown in this figure using the clusters formed by the Ti ions and the nearest neighbor cations in (a). Deformed Zr4d states in –Ti–O–Zr–O–Ti– network are shown by dotted curve and non-deformed Zr4d states are also shown by broken curve.

model, taking account of the relationship between local crystal and electronic structure was proposed using a cluster constructed by the Ti ion and the first neighboring Zr ions in TD-YSZs. Existence of Y^{3+} ions in TD-YSZ are neglected, because the electronic transport properties and E_g^{σ} values are independent of $YO_{1.5}$ concentration. From the experimental results, the new electron conduction path is suggested to be formed in TD-YSZs when the clusters are connected by one or more common Zr ions that correspond to the higher concentration of the threshold for third nearest neighbors.

Region (II) is found to be in the range between x_{III} and x_I. Schematic illustration of (100) plane of ZrO_2 with fluorite structure and the distribution of the clusters are shown in Fig. 7a where the paths are connected by clusters sharing one or two common Zr ions. The network formed in the x regions from x_{III} to x_{II} and between x_{II} and x_I is the same (–Ti–O–Zr–O–Ti–), and the difference is whether or not the

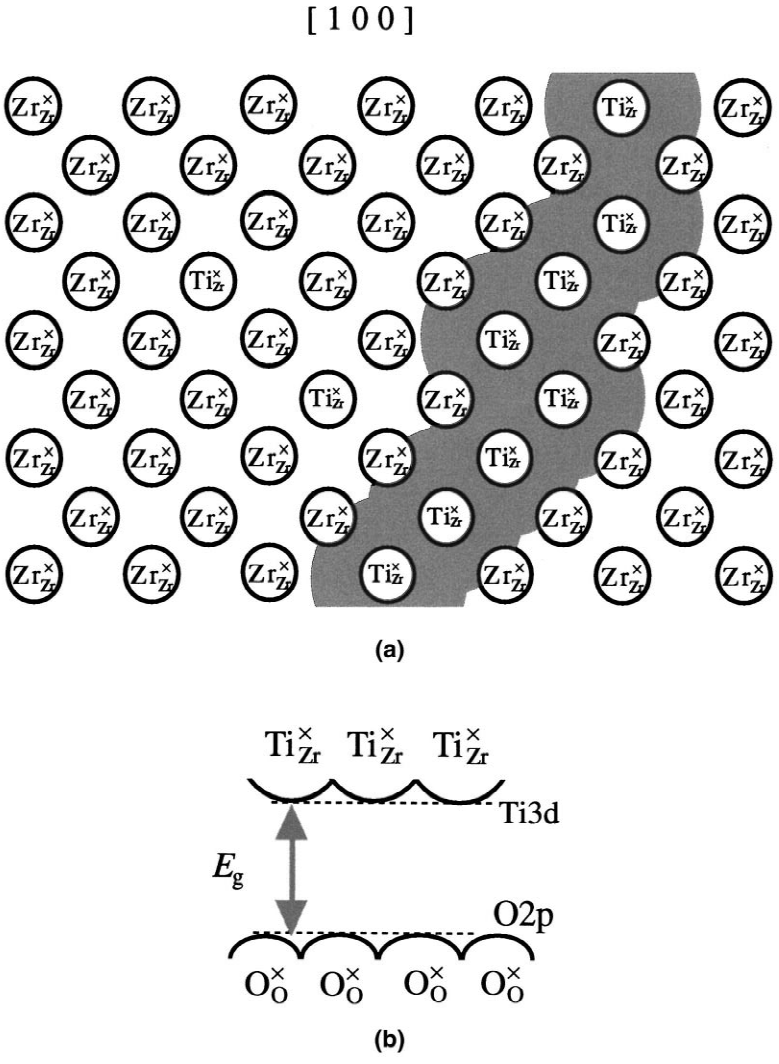

Fig. 8. Schematic illustration of (a) the cation coordination on (100) plane and (b) the electronic structure in this path. Percolation path of first nearest neighbors is also shown in this figure using the clusters formed by the Ti ions and the nearest neighbor cations.

network is collinear or noncollinear. In this paths, electrons on Ti ions have to migrate over the Zr ion from a Ti ion to the nearest Ti ones. It seems reasonable that Zr4d orbital in –Ti–O–Zr–O–Ti– network is deformed due to the different ionic radii between the Ti and Zr ions as shown in Fig. 7b. Because the deformed Zr4d is the saddle point of the migration path for electrons, the apparent activation energy for the migration of electrons will decrease. In this case Ti3d states works as a local defect band and therefore, E_g^{σ} in region (II) is smaller than that of non-doped YSZ.

In region (III), percolation paths connected by the first nearest neighbor Ti ions are formed as shown in Fig. 8a with the electronic structure of this paths in Fig. 8b. The electrons can migrate only on Ti3d band and therefore, the Ti3d states work as a conduction band in this region.

5. Conclusion

The σ_n° values increase with increasing TiO_2 concentration, while the activation energy (E_{an}) decrease by the TiO_2 doping. In contrast to the σ_n°, the σ_p° and E_{ap} are almost independent of the TiO_2 content. The unoccupied Ti3d states are found to form at the lower edge of the unoccupied Zr4d states for 5TD- and 10TD-YSZ by the XAS measurements, and the gap energy of the Zr4d states and Ti3d states show good agreement with the E_g^{σ} difference between the values of non-doped YSZ and 5TD- or 10TD-YSZ. Variation of the E_g^{σ} with x was discussed using the modified percolation model taking account of the relationship between the local crystal structure and electronic structure.

References

[1] S.S. Liou, W.L. Worrell, Appl. Phys. A49 (1989) 25.
[2] H. Naito, H. Arashi, Solid State Ionics 53–56 (1992) 436.
[3] T. Lindegaard, C. Clausen, M. Mogensen, in: F.W. Poulsen, J.J. Bentzen, T. Jacobsen, E. Skou, M.J. Østergárd (Eds.), Proc. 14th Riso Int. Symp. on Materials Science, Riso Natl. Lab, Roskilde, 1993, p. 311.
[4] K. Kobayashi, K. Kato, T. Kawashima, S. Yamaguchi, Y. Iguchi, J. Ceram. Soc. Jpn. 106 (1998) 1073, (in Japanese).
[5] K. Kobayashi, Y. Kai, S. Yamaguchi, N. Fukatsu, T. Kawashima, Y. Iguchi, Solid State Ionics 93 (1997) 193.
[6] K. Kobayashi, Y. Kai, S. Yamaguchi, T. Kawashima, Y. Iguchi, Korean J. Ceram. 4 (1998) 114.
[7] U. Vohrer, H.-D. Wiemhöfer, W. Göpel, B.A. van Hassel, A.J. Burggraaf, Solid State Ionics 59 (1993) 141.
[8] K.E. Swider, W.L. Worrell, J. Electrochem. Soc. 143 (1996) 3706.
[9] K. Kobayashi, K. Kato, K. Terabe, S. Yamaguchi, Y. Iguchi, J. Ceram. Soc. Jpn. 106 (1998) 860, (in Japanese).
[10] J. Mizusaki, K. Fueki, Rev. Chim. Miner. 17 (1980) 356.
[11] C. Wagner, in: Proc. 7th Int. Conf. Electrochem. Thermodyn. Kinetics, Lindau 1955, Butterworth, London, 1956, p. 361.
[12] A.V. Boris, S.I. Bredikhin, Solid State Ionics 40/41 (1990) 269.
[13] S. Bredikhin, T. Hattori, M. Ishigame, Phys. Rev. B 50 (1994) 2444.
[14] F.A. Kröger, H. Vink, in: F. Seitz, D. Turnbull (Eds.), Solid State Physics, Academic Press, Orlando, FL, 1956, p. 307.
[15] L.D. Burke, H. Rickert, R. Steiner, Z. Physk. Chem. NF 74 (1971) 146.
[16] W. Weppner, Z. Naturforsch. 31a (1976) 1336.
[17] M. Kleitz, E. Fernandez, J. Fouleiter, P. Fray, Advances in Ceramics 3, Science and Technology of Zirconia I., 1981, p. 349.
[18] A. Kopp, H. Näfe, W. Weppner, Solid State Ionics 53–56 (1992) 853.
[19] A. Kopp, H. Näfe, W. Weppner, P. Kountouros, H. Schubert, in: S.P.S. Badwal, M.J. Bannister, R.H.J. Hannink (Eds.), Proceedings of the International Conference on Zirconia V, Technomic, Lancaster, PA, 1993, p. 567.
[20] R.N. Blumenthal, J. Coburn, J. Baukus, W.M. Hirth, J. Phys. Chem. Solid. 27 (1966) 643.
[21] U. Vohrer, H.-D. Wiemhöfer, W. Göpel, Sensors Actuators B 4 (1991) 411.
[22] N. Nicoloso, R.I. Merino, H. Yugami, J. Maier, in: Proc. 1st Int. Symp. Ceram. Membranes PV95-24, 1997, p. 106.